Synthesis and characterization of Al_2O_3 and SiO_2 films with fluoropolymer content using rf-plasma magnetron sputtering technique

Mohammad Islam[a)]
Centre for Chemical Engineering and Material Sciences (CCE&MS), National University of Sciences & Technology (NUST), Islamabad 44000, Pakistan

Osman T. Inal
Department of Materials and Metallurgical Engineering, New Mexico Institute of Mining and Technology, Socorro, New Mexico 87801

(Received 18 July 2007; accepted 10 December 2007; published 17 January 2008)

Pure and molecularly mixed inorganic films for protection against atomic oxygen in lower earth orbit were prepared using radio-frequency (rf) plasma magnetron sputtering technique. Alumina (Al_2O_3) and silica (SiO_2) films with average grain size in the range of 30–80 nm and fully dense or dense columnar structure were synthesized under different conditions of pressure and power. Simultaneous oxide sputtering and plasma polymerization (PP) of hexafluoropropylene (HFP) led to the formation of molecularly mixed films with fluoropolymer content. The degree of plasma polymerization was strongly influenced by total chamber pressure and the argon to HFP molar ratio (n_{Ar}/n_M). An order of magnitude increase in pressure due to argon during codeposition changed the plasma-polymerization mechanism from radical-chain- to radical-radical-type processes. Subsequently, a shift from linear CH_2 group based chain polymerization to highly disordered fluoropolymer content with branching and cross-linking was observed. Fourier transform infrared spectroscopy studies revealed chemical interaction between depositing SiO_2 and PP-HFP through appearance of absorption bands characteristic of Si—F stretching and expansion of SiO_2 network. The relative amount and composition of plasma-polymerized fluoropolymer in such films can be controlled by changing argon to HFP flow ratio, total chamber pressure, and applied power. These films offer great potential for use as protective coatings in aerospace applications. © *2008 American Vacuum Society.* [DOI: 10.1116/1.2831503]

I. INTRODUCTION

Kapton is used as flexible substrate for lightweight, high power solar arrays in low earth orbit (LEO). The incident flux of atomic oxygen (AO) for normal and solar facing surfaces causes oxidation leading to breakup of bonds within its backbone, formation of volatile low molecular weight fragments, and evolution of CO and CO_2 presumably from imide ring decomposition, with subsequent erosion yield of $\sim 3 \times 10^{-24}$ cm^3/atom.[1] Thus, unprotected Kapton undergoes mass loss at a rate that is approximately 50 times more than the tolerance limit set for reasonable array lifetime expectancy.[2] This necessitates the use of protective films against AO attack in LEO environment of both shuttle and space station. Such films must meet stringent criteria based on processing, physical properties, and service conditions.[3]

Several materials explored for Kapton protection fall into three major groups, namely, inorganic, organic polymer, and molecularly mixed inorganic films. The inorganic films (Al_2O_3, ITO, SiN_xH_y, and SiO_2) show no degradation over extended exposure to AO attack through establishment of an impervious inert surface layer. The brittle nature of these films, however, places limitations on their use due to possible film cracking during postfabrication bending and deployment. The inorganic polymer films exhibit limitations due to poor substrate adhesion (hexamethyldisilazane, HMDS-TFE),[4] long-term exposure instability (polysiloxane, polyimide),[5] or surface contamination during exposure through release, transport, and subsequent condensation of polymeric scission fragments (silicone, siloxane).[6,7] The molecularly mixed inorganic films are composed of inorganic matrix with some fluoropolymer content to offer flexibility during bending and other postfabrication handling processes. Since the fluoropolymer itself is not durable and forms cone-like or carpet-type morphology upon exposure to AO flux,[8] its content in the inorganic film must be optimized for effective protection against prolonged LEO exposure.

The molecularly mixed inorganic films can be produced by combining physical vapor deposition process with plasma polymerization of a fluorocarbon monomer gas. Synthesis and characterization of SiO_2-fluoropolymer films from ion-beam sputtering,[1] dc and high frequency reactive magnetron sputtering[4] and rf-plasma sputtering using a hybrid SiO_2/polytetrafluoroethylene target[7] have been reported in literature. The ion-beam sputtering and dc reactive sputtering techniques have issues with scalability and process control. In the latter case, less than stoichiometric films are produced which become fully oxidized upon initial exposure to LEO.

This article presents work on synthesis and characterization of inorganic oxide as well as molecularly mixed films based on Al_2O_3 and SiO_2. Initially, processing conditions were optimized to obtain Al_2O_3 and SiO_2 films with submi-

a)Electronic mail: mohammad.islam@gmail.com

TABLE I. Processing conditions for pure and molecularly-mixed oxide films.

Pure oxide films					
Al_2O_3 films			SiO_2 films		
Sample	Power (W)	Pressure (mTorr)	Sample	Power (W)	Pressure (mTorr)
A-0	100	2	S-0	100	2
A-1	200	2	S-1	200	2
A-2	100	20	S-2	100	20
A-3	200	20	S-3	200	20

Molecularly mixed oxide films					
Sputter deposition			Plasma polymerization		
Sample	Power (W)	Pressure (mTorr)	n_M/n_{Ar}	Power (W)	Pressure (mTorr)
			Al_2O_3/PP-HFP		
MA-0a	100	2	0.68	100	6
MA-2a	100	20	1.14	100	87
			SiO_2/PP-HFP		
MS-0a	100	2	2.00	100	11
MS-2a	100	20	1.00	100	78
MS-2b	100	20	0.80	100	67

cron grain size and minimum defect density using radio-frequency (rf) magnetron sputtering technique. The deposition unit was then modified to achieve codeposition of Al_2O_3 or SiO_2 with plasma polymerized hexafluoropropylene (PP-HFP). The results obtained from structural and chemical characterizations of the films so produced are presented and discussed.

II. EXPERIMENT

A. Synthesis of pure inorganic films

The configuration of the rf-plasma magnetron sputtering system used for this study is described elsewhere.[9] Using high-purity oxide targets (AJA International), alumina (Al_2O_3) and silica (SiO_2) films were prepared under different conditions of applied power (P) and chamber pressure (p). Other processing variables such as argon gas flow rate (F_{Ar}), substrate temperature (T_s), target-to-substrate separation ($d_{T\text{-}s}$), and film deposition time (t) were kept at their respective values of 10 SCCM (SCCM denotes cubic centimeter per minute at STP), 300 K, 10 cm, and 4.0 h.

B. Synthesis of molecularly mixed films

The deposition system was modified to obtain inorganic Al_2O_3 or SiO_2 films with PP-HFP content. This was accomplished by introducing an inlet stream of HFP monomer gas (Aldrich, 295388-300G) as precursor for plasma polymerization. The rf power used for sputter deposition of pure oxide films also served as plasma-polymerization source during codeposition process. The choice of HFP [$F_2C{=}CF{-}CF_3$] was made due to its low F/C ratio of 2 and the presence of unsaturated C=C bond. The low F/C value limits release of atomic fluorine that is integral to plasma etching reaction, whereas an unsaturated monomer causes higher yield of diradical fragments that are more likely to participate in plasma-polymerization reaction.[10]

Due to low sputtering yields for oxide targets, sputter deposition was carried out during the entire length of film synthesis routine. At regular intervals, HFP gas was introduced into deposition chamber at 3.4 SCCM. Each codeposition period lasted 5 min during which the respective values of P and F_{Ar} were kept unchanged at 100 W and 10 SCCM, while recording any changes in total pressure. The plasma-polymerization process was carried out in 4 cycles. The feed composition during codeposition process was expressed in terms of molar flow ratio (n_M/n_{Ar}), which is the number of moles of monomer HFP gas relative to that of nonpolymerizable argon gas. The synthesis conditions for both pure and molecularly mixed oxide films are listed in Table I.

C. Characterization

The films were examined for growth characteristics, chemical composition. The surface topography and film cross sections were viewed using scanning electron microscopy (SEM) (JEOL 6100). For SEM studies of film cross sections, glass substrates with deposited films were cleaved from back side in order to avoid any change in as-deposited film structure. Film thickness measurements were obtained by measuring average step height of the film relative to the exposed substrate using surface profilometer (VEECO Dektak 3). Infrared spectra of the films were recorded at room temperature in the range of 4000–400 cm^{-1} using Fourier

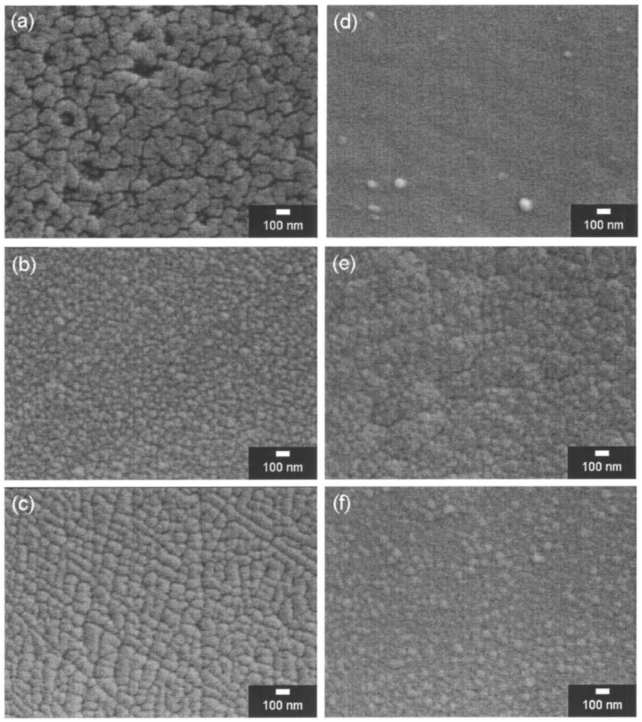

FIG. 1. High magnification view of the Al_2O_3 (A) and SiO_2 (S) films: (a) A-0; 100 W, 2 mTorr, (b) A-2; 100 W, 20 mTorr, (c) A-3; 200 W, 20 mTorr, (d) S-0; 100 W, 2 mTorr, (e) S-2; 100 W, 20 mTorr, and (f) S-3; 200 W, 20 mTorr.

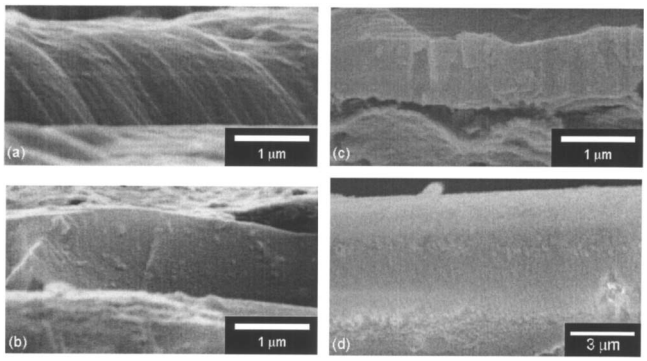

FIG. 2. High magnification SEM images of oxide film cross sections: (a) Al_2O_3; 100 W, 2 mTorr, 4 h, (b) Al_2O_3; 100 W, 20 mTorr, 2 h, (c) SiO_2; 100 W, 2 mTorr, 4 h, and (d) SiO_2; 200 W, 2 mTorr, 4 h.

transform infrared (FTIR) spectrometer (ThermoNicolet AVATOR370). The results were analyzed to investigate the extent of plasma polymerization, linear or cross-linked character of the fluoropolymer content, and any interaction between the arriving fluxes during codeposition process.

III. RESULTS AND DISCUSSION

A. Scanning electron microscopy

The SEM examination of both Al_2O_3 and SiO_2 film surfaces revealed formation of very smooth, nanocrystalline grain structure. The degree of surface roughness increased slightly with increase in chamber pressure and/or applied power. The film microstructures at high magnification are shown in Fig. 1. From the SEM image, as shown in Fig. 1(a), the average grain size was found to be ~40 nm. The presence of relatively large agglomerates, ~97 nm in size, with extensive degree of film cracking (or void formation) is believed to be caused by intense localized heating of the film due to e-beam surface interactions, thus leading to film disintegration and grain coalescence. The other Al_2O_3 films exhibited continuous, defect-free, and fine grain morphology, as evident from Figs. 1(b) and 1(c). For SiO_2 films prepared under similar set of processing conditions, the sample S-0 had an extremely smooth surface and the grain morphology could not be resolved even at 80 000× magnification. Using high magnification SEM microstructures, the average grain size for S-2 and S-3 films was found to be ~38 and 49 nm, respectively. Comparison of the microstructures revealed that deposition pressure had more significant effect on average grain size than applied power, as indicated by Figs. 1(d)–1(f).

Figure 2 shows the effect of chamber pressure and power on growth characteristics of some of the Al_2O_3 and SiO_2 film cross sections. For Al_2O_3 films, increasing the value of p from 2 to 20 mTorr changed the growth morphology from dense columnar to fully dense structure, as shown in Figs. 2(a) and 2(b). On the other hand, doubling the applied power for SiO_2 deposition demonstrated a transition in growth morphology from fully dense to dense columnar structures with an accompanying increase in deposition rate. According to the structure zone model proposed by Kelly and Arnell,[11] these dense columnar and fully dense structures belong to zones 2 and 3, respectively. At low homologous temperatures (T/T_m, where T is the substrate temperature and T_m is the melting point of the target, both in Kelvin) and in the absence of any external substrate bias, the transition in growth mechanism may be attributed to variations in target current caused by any change in p or P. The ability to form high temperature structures at low homologous temperatures has also been reported for reactively sputtered ZnO thin films.[12] From high magnification SEM images, the average column width for Al_2O_3 and SiO_2 films were estimated to be 62 and 120 nm, respectively. The average values of grain size, film thickness, and deposition rate are listed in Table II. Small amounts of argon and CO_2 have also been reported to be imbedded in the oxide films due to argon plasma and CO_2 backstreaming, respectively.[13]

The continuous sputter deposition of oxide film with intermittent codeposition cycles involving plasma polymerization of the precursor HFP molecules produced films with fluoropolymer content. The rate of PP-HFP deposition depends on simultaneously competing plasma etching and plasma-polymerization processes. With increase in P, a transition from energy starved, monomer rich to monomer starved, energy rich plasma occurs. In our case, the applied power of 100 W was carefully chosen to ensure reasonably high values of oxide sputtering yield and plasma-polymerzation rate.

TABLE II. Deposition characteristics of pure and molecularly mixed oxide films.

Sample	Grain size	Film thickness (μm)	Deposition rate (Å/min)
A-0	40 nm	1.50	61
A-1	52 nm	3.21	131
A-2	34 nm	1.95	82
A-3	71 nm	⋯	⋯
S-0	⋯	2.05	84
S-1	28 nm	4.73	197
S-2	38 nm	⋯	⋯
S-3	49 nm	2.36	96
MA-0a	45 nm, 3.6 μm	2.04	85
MA-2a	80 nm, 5.8 μm	1.23	34
MS-0a	4.1 μm	4.13	168
MS-2b	5.7 μm	6.70	279

The surface topographies of the molecularly mixed films at low and high magnifications are shown in Fig. 3. Two distinct surface topographies, representative of sputter deposition and codeposition processes were seen. In the case of Al_2O_3/PP-HFP films, plasma polymerization produced coarse grain structure with surface morphology similar to the one reported for pure PP-HFP films.[14] On the other hand, sputter deposition produced uniformly dispersed nanoparticles, $\leqslant$50 nm in size, over coarse grain structure. The increase in total chamber pressure during codeposition by an order of $\sim$1.5 indicated a corresponding increase in average nanoparticle size to $\sim$80 nm. This trend is consistent with findings for pure oxide films and underlines the effect of chamber pressure on average grain size. For SiO_2/PP-HFP films, although surface topography was similar to that seen in Al_2O_3/PP-HFP films, the absence of fine nanoparticles from sputtering indicated chemical interaction between the two depositing fluxes. Some degree of microcracking, however, was seen mostly at the grain boundry regions. Since deposition was carried out at room temperature, the role of any mismatch in the coefficient of thermal expansion between fluoropolymer content and pure SiO_2 is highly unlikely. Thus, microcrack formation may be attributed to either physical etching by argon plasma, or chemical etching arising from enhanced fluorine extraction at high power, or both.

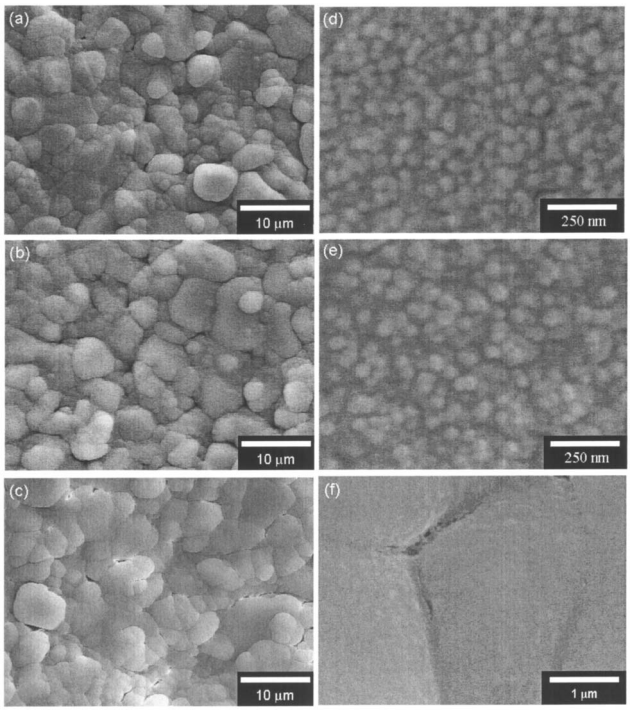

FIG. 3. Microstructures of molecularly mixed oxide film surfaces at low and high magnifications (Table I): [(a) and (d)] MA-0a, [(b) and (e)] MA-2a, and [(c) and (f)] MS-0a.

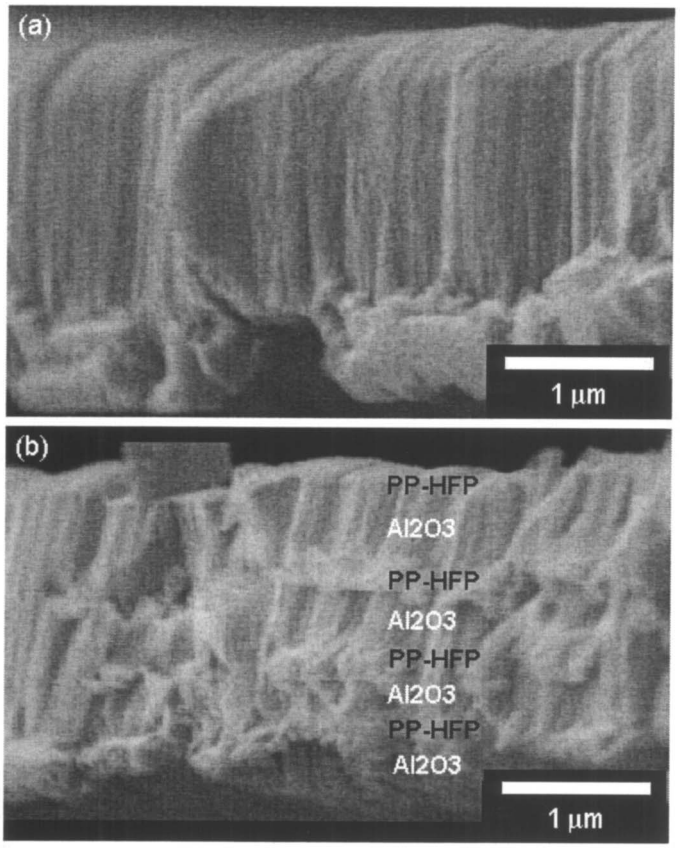

FIG. 4. Cross sections of the MA-0a film, representative of, (a) continuous columnar growth, and (b) disrupted columnar morphology.

The cross section of one of the Al_2O_3/PP-HFP films revealed regions exhibiting continuous as well as disrupted dense columnar growth, as indicated in Fig. 4. In Fig. 4(a), the film cross section revealed continuous columnar morphology with film thickness and deposition rate of $\sim$1.65 μm and 69 Å/min, respectively. On the other hand, Fig. 4(b) represented discontinous columnar structure with an estimated thickness and deposition rate of $\sim$2.04 μm and 85 Å/min, respectively. In either case, the deposition rate is higher than that of Al_2O_3 films prepared under same processing conditions. This implies incorporation of fluoropolymer

content over entire film area during codeposition process. It is speculated, however, that the nonuniform nature of arriving flux during codeposition cycle might have caused disruption of columnar growth morphology. From SEM microstructures, the deposition rates of PP-HFP content in the continuous and disrupted columnar structures were determined to be ~75 and 270 Å/min, respectively. The molar flow ratio (n_M/n_{Ar}) calculated for this experimental run was 0.68, which is relatively low and suggests the state of plasma polymerization to be monomer starved. Also, argon plasma being a well-known physical etchant with a tendency to etch through momentum transfer rather than chemical etching[15] might have contributed to film etching during codeposition. The grain structure and the degree of film roughness indicate the dominance of gas phase polymerization with some degree of argon plasma etching during codeposition.

It is noteworthy that for the same respective values of argon and HFP molar flow rates, increasing the chamber pressure during sputtering to 20 mTorr caused an increase in the HFP partial vapor pressure during codeposition. It is speculated that higher number density of argon species led to greater degree of monomer fragmentation and radical formation. Thus, for the same argon flow rate, the chamber pressure during sputtering not only affects oxide film deposition attributes but also strongly influences plasma-polymerization process in terms of fluoropolymer incorporation, degree of cross-linking, surface roughness, and overall film growth rate.

B. Fourier transform infrared spectroscopy

The film thicknesses for all samples were within the 1–20 μm range considered to be optimum for FTIR analysis. The relative height and area of the bands were examined for qualitative comparison of the analyte concentrations.[16] The FTIR spectra of the films were vertically offset for convenience. For all samples, the background peaks located at ~2340 and 2360 cm^{-1} point to the presence of trace amounts of CO_2 and water vapors. Figure 5 shows FTIR spectra of pure Al_2O_3 and Al_2O_3/PP-HFP films. In the first case, the strong IR absorption band at 780 cm^{-1} was assigned to ν_3 vibration of the isolated AlO_4 coordination group.[17] The additional bands seen in Al_2O_3/PP-HFP films were representative of different CF functionalities. Codeposition at relatively low total pressure replaced the 1000 cm^{-1} band by high intensity 960 cm^{-1} band and another 1060 cm^{-1} band positioned at its shoulder. These bands were assigned to Al—O LO (longitudinal optical) mode and CF_2 groups, respectively. The CF_2-type linear polymerization was reported for pulsed-plasma-polymerization process with on-off rf duty cycles.[18] It is likely that lack of argon species available for producing reactive intermediates, i.e., ions or radicals, tends to favor radical-chain process over radical-radical-type processes. The radical-chain polymerization process proceeds via the chemical reaction

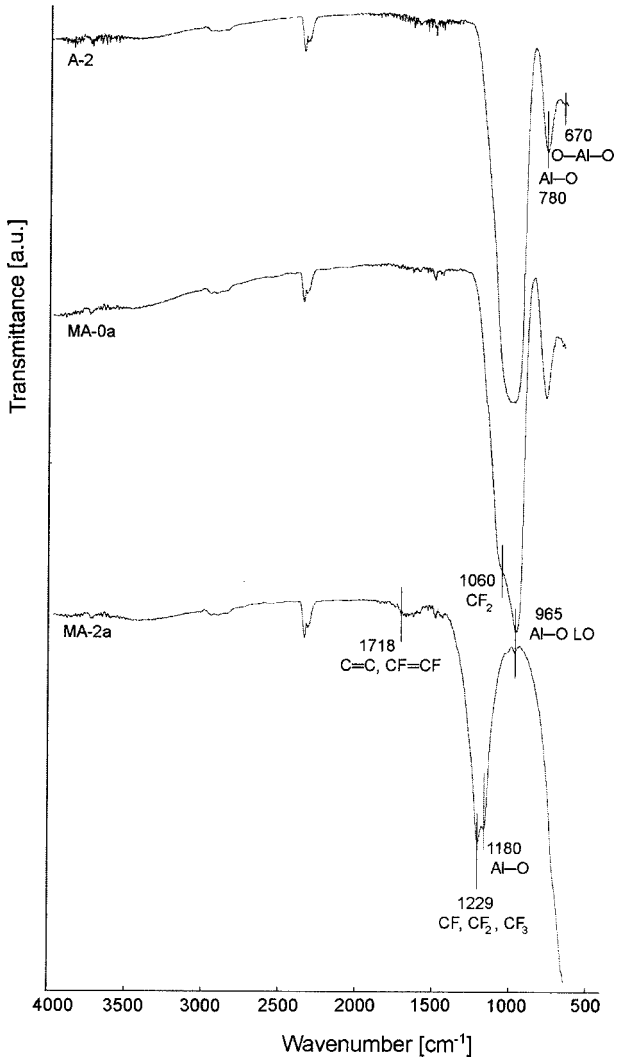

FIG. 5. FTIR spectra for pure and molecularly mixed Al_2O_3 films.

$$R + F_2C{=}CF - CF_3 \rightarrow R - CF_2 - CF - CF_2,$$

with $CF_2{=}CF$ bond scission as the preferred route for fluorocarbon plasma polymerization. The absence of $CF_2{=}CF$ band in the spectrum also testifies that due to its high energy (142 kcal/mol),[19] it is more likely to participate in the polymerization reaction.

Increasing the number density of high energy argon species in the rf-plasma glow, as in the case of much greater total pressure during codeposition, produced highly disordered films due to random branching and cross-linking. The shift in location of the band characteristic of a wide range of CF stretching frequencies such as CF, CF_2, and CF_3, from its reported value of 1229 cm^{-1} to slightly lower wave number, is associated with a slight decrease in F/C ratio and reveals formation of a roandomized structure. The strong IR band at $\leqslant$750 cm^{-1} may be due to overlapped Al—O and C—F bending mode vibrations at 650 and 737 cm^{-1}, respectively. The latter is characteristic of CF_2 wagging and C—F bending.[20] The peak due to C—F bending may arise from chain disorder, and indicate the amorphous character of the

TABLE III. Assignment of the absorption bands seen in IR spectra of pure and molecularly mixed films.

A-2	MA-0a	MA-2a	Band assignment
670	670	650	Al—O bending
		737	C—F
780	780	727	Al—O stretching
	965	965	Al—O LO (longitudinal optical)
1000			Al—O stretching mode
	1060		CF_2 group
		1180	Al—O stretching mode
		1229	CF, CF_2, and CF_3
		1718	C=C, CF=CF unsaturated bonds
		1781	$CF=CF_2$ carbon unsaturated bonds
S-2	MS-0a	MS-2a	
	737	737	C—F bending
809	804	800	Si—O bending
	930	946	Si—F stretching
964			Si—O stretching
	981	981	C—F bending
1017			Si—O—Si asymmetric stretching
	1070	1060	Si—O stretching
	1110	1110	Si—OH; silanol groups
1135			Si—O stretching mode
	1180	1180	Si—O LO_3; intensity $\propto SiO_2$ expansion
	1220	1220	CF, CF_2, and CF_3
	1718	1718	C=C, CF=CF unsaturated bonds
	1781	1781	$CF=CF_2$ unsaturated bonds

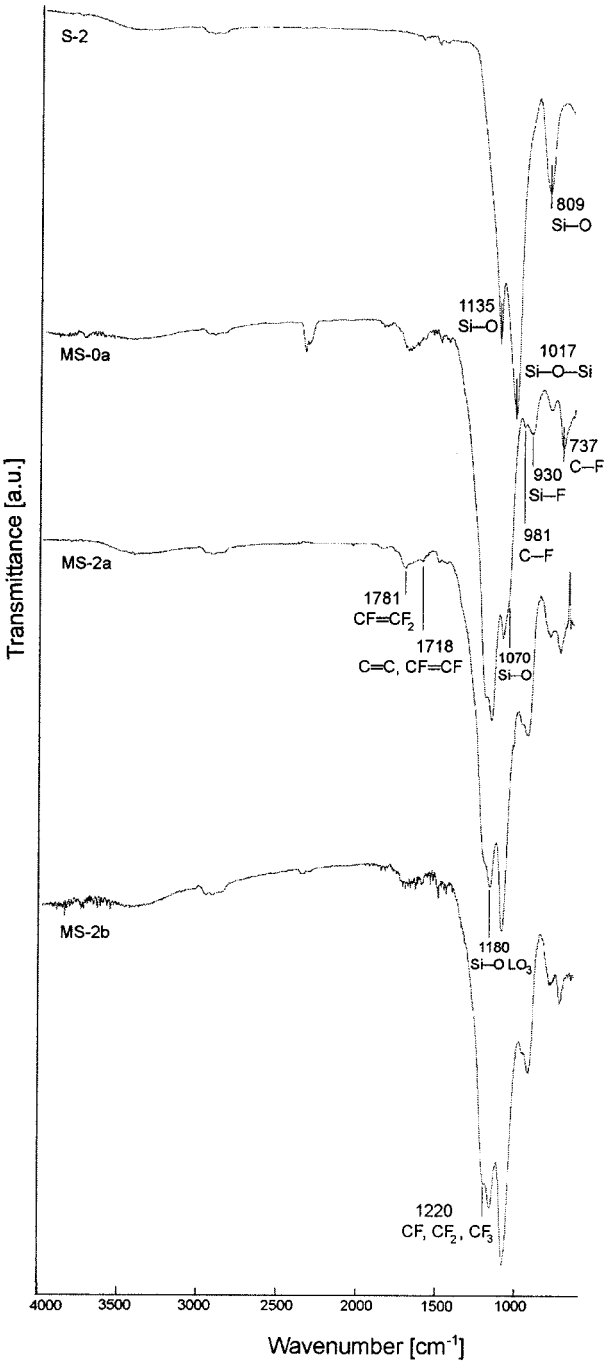

FIG. 6. FTIR spectra for pure and molecularly mixed SiO_2 films.

film with its intensity proportional to the degree of cross-linking.[21,22] The amorphous character of the films was also verified by x-ray diffraction studies. The slight decrease in F/C ratio together with the presence of unsaturated groups in the film indicate the dominance of fluorocarbon plasma polymerization via scission of C—C bond.[23] It is noteworthy that relatively high intensities of various CF frequency modes is due to the fact that film deposition was terminated immediately after last codeposition cycle. In both cases, there was no evidence of chemical interaction between sputtered Al_2O_3 and HFP based species during codeposition. Table III lists the band location with group assignment for all films.

Any increase in chamber pressure or power caused redshift or blueshift in major peak positions for pure SiO_2 films indicating variations in film density. This phenomenon is a manifestation of changes in bond characteristics such as bond angle and bond length. The incorporation of carbon and/or a high film density tends to shift the peaks to lower wave numbers (redshift). The reverse (i.e., blueshift) is true for fluorine content and/or less dense films.[24] An increase in p to 20 mTorr caused blueshift for major peaks, implying slight decrease in film density, primarily due to increased number of scattering incidents that reduce the energy of sputtered atoms and enhance oblique component in deposition flux.[25] On the other hand, redshift in dense SiO_2 films was recorded due to increased discharge current and an associated linear increase in the low-energy ion current caused by increase in P by a factor of 2.

FTIR spectra of the SiO_2 based films are shown in Fig. 6. The films were noncrystalline as demonstrated by appearance of Si—O stretching band at 1135 cm^{-1}.[13] For SiO_2/PP-HFP films, the peak with highest intensity was located at ~1180 cm^{-1} and is associated with LO_3 (longitudinal optical) vibration mode, indicating expansion of the SiO_2 network presumably due to fluorine incorporation into the films.[26] For MS-0a sample, the ~1220 cm^{-1} IR band located

at the shoulder of the 1180 cm^{-1} band is characteristic of mixed CF, CF_2, and CF_3 vibrations. The C—F bending mode vibrations resulted in IR bands at 737 and 981 cm^{-1}. The high intensity of the band at 737 cm^{-1} indicates significant degree of cross-linking during plasma-polymerization process. The overlapped absorption bands located at 1718 and 1781 cm^{-1} appear from the presence of unsaturated carbon bonds such as C═C, CF═CF, and CF═CF_2.

It was noticed that the strong band at 1015 cm^{-1} for SiO_2 films experienced a sharp decline in intensity for low total pressure SiO_2/PP-HFP film (MS-0a) and was completely absent from the spectra of high total pressure codeposited films (MS-2a, MS-2b). The CF, CF_2, and CF_3 bond formation during plasma polymerization gave rise to the peak at $\sim$1229 cm^{-1}, whereas the incorporation of fluorine into the film resulted in Si—O stretching bond frequency shift from 1060 to $\sim$1100 cm^{-1}.[23] The presence of 1140 cm^{-1} band was characteristic of Si—F stretching mode vibrations arising from chemical interaction between sputtered SiO_2 and HFP-based monomer fragments during codeposition. In the case of MS-2a and MS-2b films, however, there was a higher degree of interaction between codepositing species, as demonstrated by more intense Si—F band. A slight drop in intensity of C═C band upon increasing the total chamber pressure suggested reduced degree of cross-linking in plasma-polymerized films prepared at high total pressure. Thus, the films prepared at high deposition pressure exhibited less degree of cross-linking with a greater extent of interaction between SiO_2 and HFP during codeposition.

IV. CONCLUSIONS

For a range of processing parameters, amorphous Al_2O_3 and SiO_2 films with minimum defect density, submicron grain structure, and fully dense or dense columnar morphology can be obtained at low homologous temperatures. The film deposition rate exhibited linear dependence on applied power. The effect of pressure or power on film density was also seen in terms of red- or blueshift in bands characteristic of Si—O bending mode vibrations.

An increase in argon pressure during codeposition indicated a transition in the nature of fluoropolymer content from linear to cross-linked structure due to the change in polymerization type from predomninantly chain-radical to radical-radical processes. This demonstrates strong dependence of preferred bond scission in F_2C═CF—CF_3 on the density of argon species. The presence of two distinct surface microstructures and the absence of any bands characteristic of Al—F vibrations indicate that there was no chemical interaction between sputtered Al_2O_3 and PP-HFP. The SiO_2/PP-HFP films exhibited chemical interaction between the two arriving fluxes through appearance of Si—F stretching mode vibrations and LO_3 vibration mode due to expansion of silica network. These films offer great potential for use as protective coatings for aerospace applications.

[1]L. J. Leger, I. K. Spiker, J. F. Cuminecz, T. J. Ballentine, and J. T. Visentinc, STS Flight 5 LEO effects experiment—Background description and thin film results, AIAA-83-2631-CP (1983).
[2]I. Ritchie and H. B. Gjerde, Surf. Coat. Technol. **39–40**, 599 (1989).
[3]M. R. Reddy, N. Srinivasamurthy, and B. L. Agarwal, Surf. Coat. Technol. **58**, 1 (1993).
[4]K. M. Bilger, H. B. Gjerde, and B. L. Slater, Proceedings of the 24th International Society of Energy Conversion Eng. Conference, Washington DC, August 6–11 (1989).
[5]W. S. Slemp, B. Santos-Mason, G. F. Sykes, Jr., and W. G. Witte, Jr., Proceedings of the 23rd AIAA Aerospace Sciences Meeting, Reno, NV, January 14–17 (1985).
[6]B. A. Banks, K. K. Groh, S. Ruteledge, T. Dever, T. Stuber, and D. Hotes, Proceedings of the ASME Solar Engineering, New York (1990).
[7]D. Marvin, W. Hwang, G. Arnold, and D. Hall, Proceedings of the 23rd International Society Energy Conversion Eng. Conf., Denver, CO (1988).
[8]K. K. Groh, B. A. Banks, and R. Demko, Report No. NASA/TM-2002-211479, 2002.
[9]M. Islam, O. T. Inal, and J. R. Luke, J. Appl. Phys. **100**, 084903 (2006).
[10]R. Chen and M. S. Silverstein, J. Polym. Sci., Part A: Polym. Chem. **34**, 207 (1996).
[11]P. J. Kelly and R. D. Arnell, J. Vac. Sci. Technol. A **16**, 2858 (1998).
[12]E. Mirica, G. Cowach, and H. Du, Cryst. Growth Des. **4**, 157 (2004).
[13]W. A. Pilskin, J. Vac. Sci. Technol. **14**, 1064 (1977).
[14]R. Chen, V. Gorelik, and M. S. Silverstein, J. Appl. Polym. Sci. **56**, 615 (1995).
[15]F. D. Egitto, V. Vukanovic, and G. N. Taylor, in *Plasma Deposition, Treatment and Etching of Polymers*, edited by R. d'Agostino (Academic, New York, 1990), p. 321.
[16]B. C. Smith, *Fundamentals of Fourier Transform Infrared Spectroscopy* (CRC, Boca Raton, 1996).
[17]J. M. Saniger, N. A. Sanchez, and J. O. Flores, J. Fluorine Chem. **88**, 117 (1998).
[18]C. R. Savage, R. B. Timmons, and J. W. Lin, in *Structure-Property Relations in Polymers: Spectroscopy and Performance*, edited by C. D. Craver (American Chemical Society, Washington DC, 1993), p. 745.
[19]M. D. Garrison, R. Luginbuhl, R. M. Overney, and B. D. Ratner, Thin Solid Films **352**, 13 (1999).
[20]S. J. Limb, K. K. Gleason, D. J. Edell, and E. F. Gleason, J. Vac. Sci. Technol. A **15**, 1814 (1997).
[21]W. K. Fisher and J. C. Corelli, J. Polym. Sci., Polym. Chem. Ed. **19**, 2465 (1981).
[22]R. d'Agostino, F. Crammarosa, F. Fracassi, and F. Illuzi, in *Plasma Deposition, Treatment and Etching of Polymers*, edited R. d'Agostino (Academic, New York, 1990), p. 95.
[23]H. Yasuda, *Plasma Polymerization* (Academic, New York, 1985).
[24]Y. H. Kim, M. S. Hwang, J. Y. Kim, and Y. Lee, J. Appl. Phys. **90**, 3367 (2001).
[25]B. Window and N. Savvides, J. Vac. Sci. Technol. A **4**, 504 (1986).
[26]N. Primeau, C. Vautey, and M. Langlet, Thin Solid Films **310**, 47 (1997).